Electron. Mater. Lett., Vol. 10, No. 4 (2014), pp. 775-781
DOI: 10.1007/s13391-013-3284-y

Electro-Optical Characterization of nanoGUMBOS

A. Sarkar,[1] K. Kanakamedala,[1] M. D. Rajathadripura,[1] N. N. Jagadish,[1] P. K. S. Magut,[2] S. de Rooy,[2] S. Das,[2] B. El-Zahab,[3] I. M. Warner,[2] and T. Daniels-Race[1,4,*]

[1]Division of Electrical and Computer Engineering, School of Electrical Engineering and Computer Science, Louisiana State University, 3101 P. F. Taylor Hall, Baton Rouge, Louisiana 70803, USA
[2]Department of Chemistry, Louisiana State University, Baton Rouge, Louisiana 70803, USA
[3]Department of Mechanical and Materials Engineering, Florida International University, Miami, Florida 33174, USA
[4]Center for Computation and Technology, Louisiana State University, Baton Rouge, Louisiana 70803, USA

(received date: 1 October 2013 / accepted date: 9 December 2013 / published date: 10 July 2014)

Molecular electronics, where nanoscale organic species are utilized as active electronic components, offers a promising approach towards ultimate miniaturization and integration of hybrid electronic materials (HEMs) with traditional silicon based complementary metal oxide semiconductors (CMOS) technology. Toward this end, fundamental research studies to understand the electronic and optical properties of these molecules are of paramount importance. In this work, conductive probe atomic force microscopy (CP-AFM) and Raman spectroscopy have been performed on ionic liquid based unique organic nanoparticles derived from a Group of Uniform Materials Based on Organic Salts (GUMBOS). Aptly named as nanoGUMBOS, the material investigated in this report is Rhodamine6G tetraphenylborate ([R6G][TPB]) as has been synthesized by a room temperature facile metathesis reaction between Rhodamine 6G chloride (R6GCl) and sodium tetraphenylborate (NaTPB) followed by an ultrasonication-assisted, additive-free, re-precipitation reaction. To the best of our knowledge, the results reported herein are first-time evidence of electrical performance exhibited by [R6G][TPB] nanoGUMBOS. In conjunction with the supportive results of Raman spectra, the current-voltage (*I-V*) characteristics obtained are indicative of the potential incorporation of this unique compound in hybrid electronics with respect to potential applications in optoelectronics and chemical sensing.

Keywords: conductive probe atomic force microscopy (CP-AFM), nanoGUMBOS, raman spectroscopy, hybrid electronic materials (HEMs)

1. INTRODUCTION

Although derived from the Greek for "dwarf", ironically, "nano" and thus *nanotechnology* has presented enormous contributions to modern day electronics technology.[1,2] This interdisciplinary science examines the effect of size, in nanoscale dimension, on the material properties or structures under study. Explorative studies in molecular electronics based on single molecule or nanotube-based devices have shown promise with respect to the longevity of Moore's Law as miniaturization of silicon-based structures reaches its saturation limits. In an attempt to perpetuate standard chip functionalities and to secure a future that has been referred to as "More than Moore",[3] integration with existing silicon based CMOS technology would be the primary step for devices based on single molecules. In addition, molecular electronics as a field refers to the exploitation of organic materials as viable substitutes for electronically active layers in traditional semiconductor devices.[4,5] Our research falls within the paradigm of nano-electronics, known as *hybrid electronics*,[6,7] which essentially approaches nanotechnology from the perspective of studying the fundamental electrical characteristics of novel hybrid electronic materials (HEMs) for potential device integration. Such blending of inorganic and organic species in hybrid systems would certainly benefit from the speed and reliability of CMOS, while simultaneously offering the versatility and diverse functionalities of the nanometer device footprint.

Extensive research in different aspects of hybrid electronics has been actively pursued. To contribute to the ongoing efforts of successful integration of molecular species with traditional inorganic materials, the present work is directed toward the task of investigating an essentially new form of organic material known as GUMBOS (Group of Uniform Materials Based on Organic Salts) in order to ascertain their potential as functional components for future HEM based devices. As reported in 2008, both micro and nano sized

*Corresponding author: tdrace@lsu.edu

particles have been synthesized from GUMBOS. GUMBOS are classified as a class of solid phase materials that are composed of cations and anions similar to ionic liquids but exhibit a wider range of melting points (25°C - 250°C) than typically defined for ionic liquids (m.p. < 100°C).[8] The unique and particular interest in GUMBOS stems from their solid-state nature due to their extended range of melting points up to 250°C with respect to traditional ionic liquids. GUMBOS are extremely interesting materials in regard to ionic conductivity and thermal stability, both of which are essential for organic-inorganic materials integration. Moreover, flexible functionalities based upon the variation of either the anionic or the cationic component in its structure result in an effective combination of properties. For example, fluorescent GUMBOS can be simply synthesized by employing a fluorescent ionic dye as the cation.[9] To produce magnetic GUMBOS, $FeCl_4^-$ can be used as the paramagnetic anion.[10] In terms of morphologies, the versatility of GUMBOS is extensive as these materials have also been successfully synthesized in the form of nanoparticles/nanowires/nanorods which, in turn, have exhibited the aforementioned properties of fluorescence, magnetic susceptibility, and even antimicrobial activity. More detailed information in the synthesis methods (e.g. melt emulsion quench technique, re-precipitation, *in situ* ion exchange and hydrogel formation) and the resultant functionalities imparted to GUMBOS and nanoGUMBOS can be found in publications to date.[11-14]

These versatile properties have inspired us to investigate the electrical and spectral behavior of GUMBOS with the future goal of incorporating these unique compounds into the area of hybrid and opto-electronics. Conductive probe atomic force microscopy (CP-AFM) and Raman Spectroscopy were deemed to be the most suitable characterization techniques for this stage of our study. Since its inception by Binnig *et al.*[15] following the invention of scanning tunneling microscopy (STM) in 1981,[16,17] the immense potential of AFM as a surface characterization tool has been recognized in a multitude of research endeavors.[18-26] Recently a number of new AFM techniques (e.g. electrostatic force microscopy, scanning capacitance microscopy, scanning Kelvin probe microscopy and scanning tunneling potentiometry)[27-29] exploiting electrically conducting probes have been developed to measure electrostatic forces, charge distributions, voltage drops, capacitances and resistances on sub-100 nm scale materials in different aspects of nano-science. Conductive probe atomic force microscopy (CP-AFM) is a variation of these conductive microscopy techniques in which conducting probes are positioned with controlled load at desired points on the nanomaterial, and the resistance or *I-V* response are estimated under different experimental conditions.[28,30-32] In turn, Raman Spectroscopy (RS)[33] has emerged as one of the essential characterization techniques for comprehensive understanding of molecular structure. Due to its sensitivity to backbone structure and symmetric bonds, and non-destructive nature of interaction with the target analyte, RS is now used in numerous materials science based applications across fields ranging from chemistry,[34] biology,[35,36] and geology[37] to forensic science, art, and archeology.[38] With the development of innovative techniques like Resonance Raman Spectroscopy (RRS),[39] Tip-Enhanced Raman Spectroscopy (TERS)[40] and Surface-Enhanced Raman Spectroscopy (SERS),[41,42] the limited sensitivity has been far surpassed, and the detection limit has been now pushed down to single molecule detection, thus making RS as an ideal characterization technique for the work as reported here.

Therefore, in this study RS and CP-AFM measurements have been pursued for the first time to investigate the spectroscopic response and to deduce the *I-V* characteristics of ionic liquid-based Rhodamine6G tetraphenylborate ([R6G][TPB]) nanoGUMBOS. No prior work of such kind is known to the authors given that the GUMBOS and nanoGUMBOS qualify as virtually a "new" class of materials. Therefore, the results reported in this article are unique and contribute to a preliminary understanding of the electrical and spectral characteristics of this material.

2. MATERIALS AND INSTRUMENTATION

2.1 Synthesis of [R6G][TPB] GUMBOS and nanoGUMBOS

Literature outlining the detailed synthesis process of various GUMBOS and nanoGUMBOS can be obtained from the references stated earlier. The following briefly describes the general strategy of synthesis of [R6G][TPB] nanoparticles.[12]

The rhodamine-based GUMBOS were synthesized through a facile metathesis reaction between rhodamine 6G chloride [R6G][Cl] and sodium tetraphenylborate [Na][TPB] in a biphasic mixture of water and dichloromethane (DCM). Following the ion exchange reaction, the organic phase containing rhodamine 6G tetraphenylborate ([R6G][TPB]) GUMBOS was rinsed several times with ultrapure water (18.2 MΩ-cm) to eliminate any sodium chloride byproduct. Finally, DCM was evaporated to obtain dry [R6G][TPB].

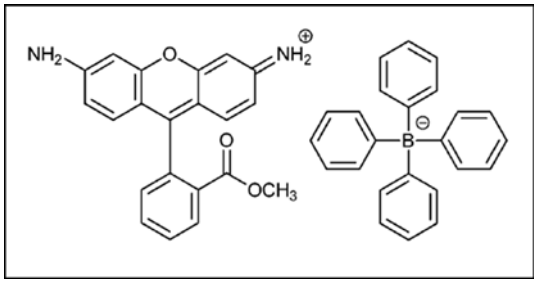

Fig. 1. Chemical structure of [R6G][TPB][13] - *Reproduced by permission of The Royal Society of Chemistry.*

The nanoGUMBOS were prepared from the GUMBOS via a modified, additive free reprecipitation method such as that used for organic nanoparticles. In this method, 100 μL of a 1 mM solution [R6G][TPB] GUMBOS dissolved in ethanol was quickly injected into 5 mL of triply deionized water in an ultrasonic bath, followed by further sonication for 5 minutes. Filtration of water and ethanol prior to preparation of the nanoGUMBOS was performed using 0.45 μm nylon membrane filters. The suspended nanoGUMBOS were then aged for 1 hour in the dark. The chemical structure of the synthesized nanoparticle is shown in Fig. 1.

2.2 Sample preparation

Glass substrates (Corning plain microscope slides, thickness ~1 mm) and silicon wafers (resistivity: 0-100 ohm-cm, thickness ~500 μm) were cleaned with warm piranha solution (H_2SO_4:H_2O_2 = 1:1) for about 30 minutes to remove any organic impurities. A thin layer of gold (thickness ~200 nm) was deposited on the glass substrates by thermal evaporation. The gold deposited glass substrates and the silicon wafers were further cleaved into smaller samples (1-1.5 × 1-1.5 cm^2) for CP-AFM and Raman spectroscopic studies.

The [R6G][TPB] nanoparticles were deposited on 2 different substrates (gold coated glass samples and silicon samples) by drop-casting method. The [R6G][TPB] nanoparticle solution was kept in the ultrasonic bath for 15 minutes prior to the deposition process to minimize the agglomeration of the particles in the solution. Approximately 10 μL of [R6G][TPB] nanoGUMBOS in aqueous solution were dispensed on the substrates. The dispensed droplet was allowed to spread out evenly on the surface and dried in ambient air for 24 hours before further characterization experiments. Also 10 μL of [R6G][TPB] GUMBOS in ethanol was drop casted on silicon samples for spectroscopic measurements.

2.3 AFM imaging and conductive-probe

The schematic diagram of the experimental set up is shown in Fig. 2. A Nano-R model atomic force microscope (AFM) from Pacific Nanotechnology (now Agilent) with a conductive tip is used for electrical characterization. The tip (DPE 14/no Al), purchased from MikroMasch, is a silicon tip with 30 nm platinum (Pt) coating. The radius is less than ~40 nm and height is ~20 - 25 μm, cone angle <40° with resonant frequency of ~160 kHz approximately and force constant of ~5.7 N/m. The conducting probe is mounted on a rectangular 3.4 × 1.6 × 0.4 mm silicon chip.

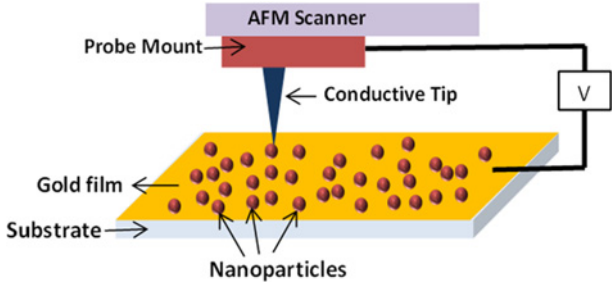

Fig. 2. Schematic diagram of conductive probe atomic force microscopy (CP-AFM) technique for electrical characterization of nanomaterials.

The AFM was operated in *contact mode* to estimate the current-voltage (*I-V*) characteristics, where the conductive tip is used as one of the electrodes with the other being the gold surface, thereby forming a metal (Pt)-particle ([R6G][TPB])-metal (Au) junction. The tests were configured by the Keithley 4200 Semiconductor Characterization System (SCS) and Keithley Interactive Test Environment (KITE) program. Prior to the *I-V* measurements, AFM images of the [R6G][TPB] nanoGUMBOS were obtained by surface scanning by Pacific Nanotechnology tip (Model: P-MCU-SICT-O) in contact mode. The AFM was interfaced with Pacific Nanotechnology SPM Cockpit software; the surface and 3D images of all the samples were obtained using NanoRule software. The tips used for all of the imaging and CP measurements were chosen carefully to minimize delamination or adsorption of the particles to the tip surface.

2.4 Raman spectroscopy

Raman spectroscopy measurements were performed using a Jobin Yvon Horiba Labram Raman spectrometer. A HeNe laser with wavelength 638.4 nm and incident power of 17 mW was used for the spectroscopic analysis. The confocal hole aperture of 200 μm and grating of 1800 lines per mm were selected during the measurement. Extended scans were performed between 600 cm^{-1} and 1800 cm^{-1} for best results. The exposure time during an extended scanning for each spectral window (acquisition time) was set to be 5 seconds with the accumulation number of 5. A 100X objective from Olympus was used for focusing and during scanning. The acquired Raman spectra were corrected using an 8-order polynomial fitting curve of fluorescence backgrounds, which was performed using the LabSpec software.

3. RESULTS AND DISCUSSION

3.1 AFM imaging of [R6G][TPB] on gold surface

The AFM images and the height profiles of the deposited nanoparticles, obtained prior to the conductive probe experiments, are shown in Fig. 3(a). A suitable area from Fig. 3(a) was selected and scanned (area: 5 μm × 5 μm) to obtain the magnified image of the particles. As can be noted in Fig. 3(b), the drop casting - air drying method leads to aggregation of the particles on the gold surface. Therefore depending on the nature of their agglomeration, the particles exhibit a wide distribution in their dimensions with the diameter values ranging between 200 nm to 500 nm

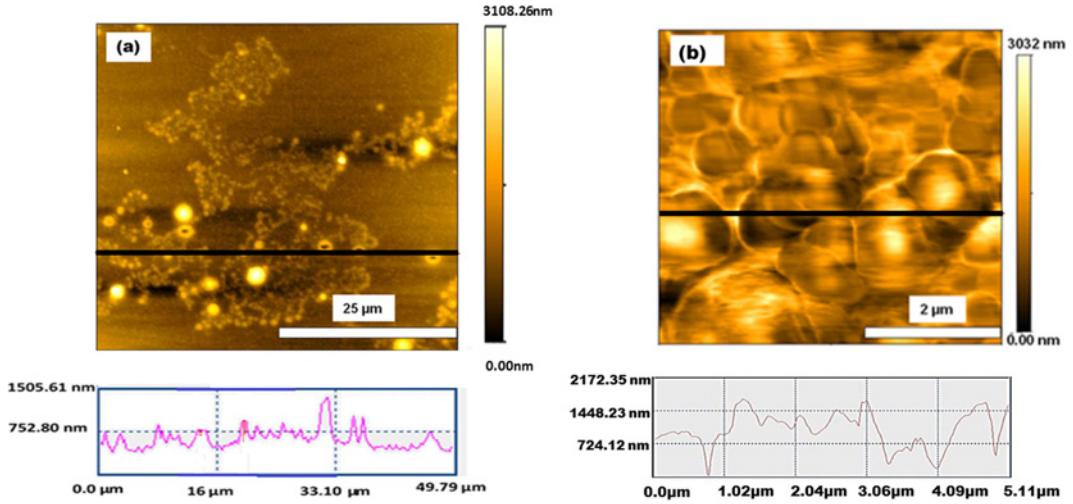

Fig. 3. Atomic Force Microscopy (AFM) images of [R6G][TPB] nanoGUMBOS (a) topographic image of the drop casted [R6G][TPB] nanoparticles on gold surface (scan area: 50 μm × 50 μm); (b) magnified image of the nanoparticles (scan area: 5 μm × 5 μm).

(estimated average value of ~300 nm). The observed height profiles, obtained during the image acquisition scanning as indicated by the black line in the AFM images, are also presented with each figure. Both the magnified AFM image and variation in height profiles, thus, depict the discontinuity in surface coverage, random orientation and stacked nature of the ensembles of [R6G][TPB] nanoparticles. The agglomeration of the functional nanoparticles in drop casted samples has been a challenging issue in material research which, in general, leads to variation in the measured data and affects the reproducibility of the characterization methods and has been mentioned in the following section.

3.2 CP-AFM results of [R6G][TPB] particles on gold surface

As substantiated by the AFM images, the drop casted and air dried samples show aggregates of nanoGUMBOS, with variations in orientations, size and non-uniform surface coverage on the gold substrate. Therefore, the CP-AFM results are dominated by the varying distributions of particle sizes and disordered aggregates or ensembles at different locations on the samples. Figure 4 depicts the current-voltage (*I-V*) curve of the nanoGUMBOS in a conductive probe configuration at different locations. The magnitude of the current through the Au-[R6G][TPB]-Pt junction is observed to vary between 10^{-6} A to10^{-7} A. As can be noted in the figure, the conductivity values at different locations on the sample are strongly influenced by the morphological variations of the ensembles of [R6G][TPB] nanoparticles. The variations can be primarily attributed to the differences in thickness due to the random, non-uniform agglomeration of the nanoparticles following the drop-casting method and eventual drying process. Additionally, for all the curves, the current increases almost monotonically as the tip voltages

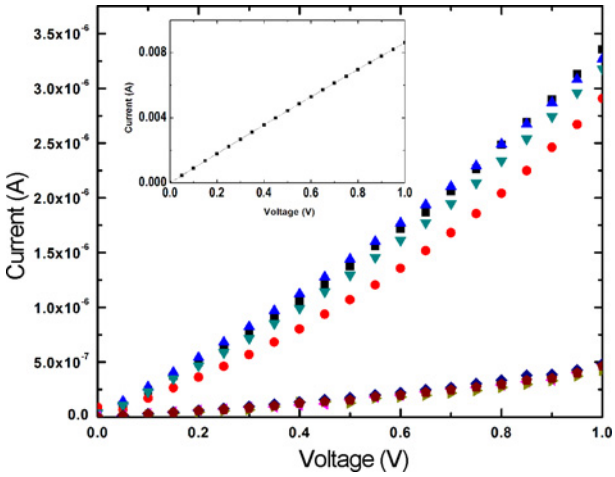

Fig. 4. Current-voltage (*I-V*) curve of the [R6G][TPB] nanoGUMBOS after conductive probe atomic force microscopy (the voltage is swept between 0 to +1 V).

are swept from 0 V to +1 V at an increment of 0.05 V. The non-linearity in the *I-V* relationship obtained by CP-AFM technique, as can be noted here also, has been reported to be a sensitive function of a number of factors, e.g. the nature of particle aggregation, interaction at the nanoparticle-substrate interface and injection of charges (or, flow of current due to electron tunneling) through the tip-nanoparticle junction barrier.[29] The average junction resistance calculated from the curves range between 0.3 MΩ to 3 MΩ. The current values obtained from Au film without the nanoGUMBOS (as shown in the inset in Fig. 4) are in the order of 10^{-3} A and shows the expected increasing trend linearly with increasing voltage as per basic Ohm's law. The imaging and electrical characterization experiments were performed with extreme caution to minimize unwanted damage or peeling off the

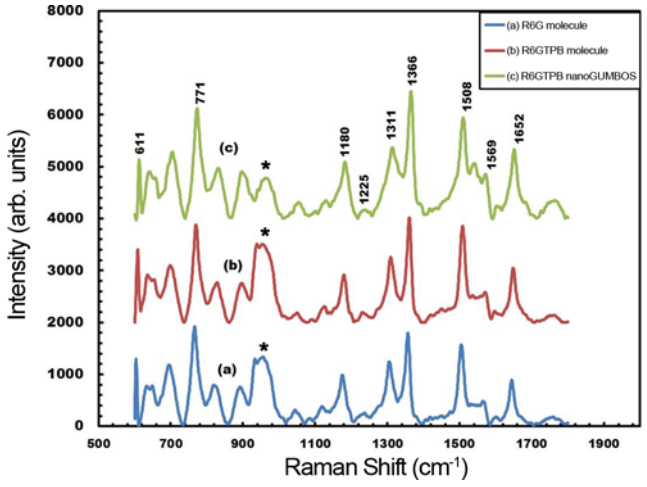

Fig. 5. Raman spectra of R6G molecules (a) (in blue), [R6G][TPB] GUMBOS (b) (in red) and [R6G][TPB] nanoGUMBOS (c) (in green) on silicon substrates showing similar peak assignments without significant variation (The acquired spectra of [R6G][TPB] GUMBOS and [R6G][TPB] nanoGUMBOS were upshifted for clarity).

Table 1. Assignment of Raman peaks of the [R6G][TPB] nanoGUMBOS.

Raman Shift (cm^{-1})	Assignment of the peaks
611	C-C-C ring in plane bending
771	C-H out-of-plane bending
1180	C-H in plane bending
1225	C-O-C stretching
1311	Aromatic C-C stretching
1311	Aromatic C-C stretching
1366	Aromatic C-C stretching
1508	Aromatic C-C stretching
1569	Aromatic C-C stretching
1652	Aromatic C-C stretching

particles from the substrate after the measurements.

3.3 Raman spectroscopic results

The acquired Raman spectra of [R6G][TPB] GUMBOS and [R6G][TPB] nanoGUMBOS on a silicon surface, were compared with the one obtained from rhodamine 6G (R6G) molecules. An aqueous solution of rhodamine 6G (chemical formula: $C_{28}H_{31}N_2O_3Cl$, molecular weight: 479.01 gm) with 20×10^{-6} M (20 μM) concentration was prepared as a reference sample. About ~10 μL of the prepared R6G solution was drop casted on silicon substrates and air dried for 24 hours. Figure 5 represents the spectroscopic results. As has been pointed out in the experimental section, the R6G based GUMBOS were prepared by simple ion exchange reaction between [R6G][Cl] and [Na][TPB]. Also, since the nanoparticles are formed due to hydrophobic interactions in the aqueous medium, it is expected that the Raman spectra of these synthesized materials would not be significantly different from the traditional R6G spectra in nature. As can be seen from the figure, the spectra of [R6G][TPB] GUMBOS and nanoGUMBOS (indicated by (b) and (c) respectively in the figure) matched with the traditional R6G Raman spectra (indicated by (a)) without any noticeable variation. (The intensity scale for the GUMBOS (b) and nanoGUMBOS (c) is upshifted for better clarity). The curves show active vibrational peaks at similar wavenumbers (or frequency shift) between 600 cm^{-1} and 1800 cm^{-1} for all the three samples. The spectra show strong peaks at 611, 771, 1180, 1311, 1366, 1508, 1652 cm^{-1} and relatively weak peaks at 1225 cm^{-1} and 1569 cm^{-1}. As summarized in Table 1, 611 cm^{-1} can be attributed to the C-C-C ring in plane bending vibration, 771 cm^{-1} represents the C-H out-of-plane vibration mode, 1180 cm^{-1} shows the C-H in plane bending, and 1225 cm^{-1} indicates the C-O-C stretching mode of the molecular vibration. Strong signals at 1318, 1366, 1508 and 1652 cm^{-1} are assigned to the numerous aromatic stretching vibrations. The peak around 960 cm^{-1} (denoted by the symbol star (*) in Fig. 5) is attributed to the second order Raman peak of the underlying silicon substrate. Table 1 shows the summary of the assignment of peaks obtained on [R6G][TPB] nanoparticles. The intensity of the signature peaks also yielded values of similar magnitude for all the three types of R6G samples with the same concentration. Therefore, it can be concluded that the metathesis synthesis approach during preparation of rhodamine based GUMBOS and the subsequent ultrasonic processing in the re-precipitation method for the nanoGUMBOS synthesis did not alter the chemical composition or induce significant modification in the vibrational nature of the rhodamine structure. The ability to preserve the spectral features of these unique nanomaterials without significant alteration in the primary dye's vibrational structure by the template free, anion exchange synthesis approach, as reported in this study, is an exciting development. Table 2 represents the comparative results (wavenumber and intensity in arbitrary units) of the strong peaks of R6G, [R6G][TPB] GUMBOS and [R6G][TPB] nanoGUMBOS spectra acquired after extensive scanning. The results corroborate the expected vibrational nature of the molecular structure of the synthesized nanoparticles.

4. CONCLUSIONS AND FUTURE WORK

Atomic force microscopic imaging and conductive probe experiments have been successfully performed, for the first time, on ionic liquid based unique nanoparticles, known as nanoGUMBOS. The AFM images indicate the particle diameter to be ~300 nm, and the electrical characterization by CP-AFM resulted in current values of ~10^{-6} - 10^{-7}A when scanned from 0 V to +1 V. The effects of particle aggregation

Table 2. Comparative results indicating similar vibrational attributes of the strong Raman peaks in R6G, [R6G][TPB] GUMBOS and [R6G][TPB] nanoGUMBOS.

R6G		[R6G][TPB]GUMBOS		[R6G][TPB] nanoGUMBOS		
Wavenumber (cm^{-1})	Intensity (arb. units)	Wavenumber (cm^{-1})	Intensity (arb. units)	Wavenumber (cm^{-1})	Intensity (arb. units)	Assignment of Raman Peaks
607.7	1257.12	608.3	1340.26	611.2	1122.32	C-C-C ring in plane bending
768.07	1903.34	769.9	1868.5	771.7	2104.34	C-H out-of-plane bending
1174.7	954.15	1178.6	897.39	1180.62	1057.03	C-H in plane bending
1307	1213.73	1310.77	1231.51	1311.3	1341.91	Aromatic C-C stretching
1358.9	1769.21	1359.69	1994.28	1361.3	2397.25	Aromatic C-C stretching
1506	1532.91	1507.38	1847.49	1508.31	1918.11	Aromatic C-C stretching
1644.08	871.83	1646.77	1022.8	1649.54	1302.75	Aromatic C-C stretching

and orientation, following the drop casting method, in the obtained *I-V* curves have also been reported. The calculated values of the junction resistance in the order of 0.3 - 3 MΩ are typical for organic-metal junctions. However, the obvious benefit of using the nanoGUMBOS in electronic applications in lieu of other organic materials remain in the ease of synthesis of these nanoparticles from their parent compounds, high thermal stability and flexible functionalities due to the variation of either the anionic or the cationic constituent in their structure. Optical characterization of GUMBOS and the GUMBOS based nanoparticles has been also accomplished using Raman Spectroscopy. The spectroscopic results have been presented to gain a better understanding of the C-C, C-H and aromatic stretching modes and to correlate the active peaks with the vibrational nature of the nanoparticle structure. Information of this form is important for not only structural elucidation but, in turn, may be of use to the studies of different phenomena (i.e.-electron phonon interactions) important to future HEMs device development.

In this communication, we are excited to bring forth first-time data in regard to the electrical and spectroscopic behavior of a virtually new class of materials. As to future work in this research endeavor, detailed theoretical simulation involving electron tunneling model through the tip-nanoparticle junction would be performed to comprehend the non-linearity of the *I-V* curve in greater depth. Comparative studies with respect to conductivity values at higher applied voltages (both positive and negative) between the ionic liquid based GUMBOS and nanoGUMBOS can also be undertaken as an exciting explorative future work. Extensive studies are underway to optimize suitable deposition methods to avoid the unwanted effects of drop casting. The work, reported here, will be extended further to study the *I-V* nanoparticle thin film with uniform surface coverage on various substrates as desired in dye-based optoelectronic applications like lasers, waveguides and in chemical sensing devices.

ACKNOWLEDGEMENTS

The authors wish to thank the Louisiana Board of Regents (LEQSF 2011-RD-A-07), NASA (DART-44), Dr. K. M. Johnson (AES Corporation), and the LSU Division of Electrical & Computer Engineering's Electronic Materials and Devices Laboratory for partial support of this work. The LSU Department of Chemistry authors gratefully thank the National Science Foundation (grant number: CHE0911118) for support of this work.

REFERENCES

1. L. E. Foster, *Nanotechnology: Science, Innovation, and Opportunity*, 1st ed., Prentice Hall (2005).
2. B. Yu and M. Meyyappan, *Solid-State Electron*. **50**, 536 (2006).
3. G. E. Moore, *Proc. of IEEE*, **86**, 82 (1998).
4. J. R. Heath, *Annu. Rev. Mater. Res*. **39**, 1 (2009).
5. H. Iijima, K. Kimura, T. Sakai, A. Uchimura, T. Shimizu, H. Ueno, T. Natori, Y. Koezuka, and Y. Wei, *Supramol. Sci*. **5**, 723 (1998).
6. T. Daniels-Race, in *Bull. Am. Phys. Soc.*, American Physical Society (2008).
7. C. Joachim, J. K. Gimzewski, and A. Aviram, *Nature* **408**, 541 (2000).
8. A. Tesfai, B. El-Zahab, D. K. Bwambok, G. A. Baker, S. O. Fakayode, M. Lowry, and I. M. Warner, *Nano Lett*. **8**, 897 (2008).
9. S. Das, D. Bwambok, B. El-Zahab, J. Monk, S. L. de Rooy, S. Challa, M. Li, F. R. Hung, G. A. Baker, and I. M. Warner, *Langmuir ACS J. Surfaces Colloids* **26**, 12867 (2010).
10. A. Tesfai, B. El-Zahab, A. T. Kelley, M. Li, J. C. Garno, G. A. Baker, and I. M. Warner, *ACS Nano* **3**, 3244 (2009).
11. A. N. Jordan, S. Das, N. Siraj, S. L. de Rooy, M. Li, B. El-Zahab, L. Chandler, G. A. Baker, and I. M. Warner, *Nanoscale* **4**, 5031 (2012).
12. S. L. de Rooy, B. El-Zahab, M. Li, S. Das, E. Broering, L.

Chandler, and I. M. Warner, *Chem. Commun*. **47**, 8916 (2011).
13. D. K. Bwambok, B. El-Zahab, S. K. Challa, M. Li, L. Chandler, G. A. Baker, and I. M. Warner, *ACS Nano* **3**, 3854 (2009).
14. J. C. Dumke, B. El-Zahab, S. Challa, S. Das, L. Chandler, M. Tolocka, D. J. Hayes, and I. M. Warner, *Langmuir* **26**, 15599 (2010).
15. G. Binnig, C. F. Quate, and Ch. Gerber, *Phys. Rev. Lett*. **56**, 930 (1986).
16. G. Binnig, H. Rohrer, C. Gerber, and E. Weibel, *Phys. Rev. Lett*. **49**, 57 (1982).
17. D. M. Eigler and E. K. Schweizer, *Nature* **344**, 524 (1990).
18. S. Liu and Y. Wang, *Scanning* **32**, 61 (2010).
19. S. Bandyopadhyay, S. K. Samudrala, A. K. Bhowmick, and S. K. Gupta, in *Funct. Nanostructures*, Springer, New York, pp. 504-568 (2008).
20. H. Yang, Y. Wang, S. Lai, H. An, Y. Li, and F. Chen, *J. Food Sci.* **72**, R65 (2007).
21. A. Alessandrini, *Meas. Sci. Technol*. **16**, R65 (2005).
22. N. Jalili, *Mechatronics*, **14**, 907 (2004).
23. K. S. Birdi, *Scanning Probe Microscopes-Applications in Science and Technology,* CRC Press, New York (2003).
24. N. H. T. S. Kasas, *Int. J. Imaging Syst. Technol*. **8**, 151 (1997).
25. T. Ushiki, J. Hitomi, S. Ogura, T. Umemoto, and M. Shigeno, *Arch. Histol. Cytol*. **59**, 421 (1996).
26. H. Hansma and J. Hoh, *Annu. Rev. Biophys. Biomol. Struct.* **23**, 115 (1994).
27. E. Meyer, H. J. Hug, and R. Bennewitz, *Scanning Probe Microscopy: The Lab on a Tip*, Springer (2003).
28. T. W. Kelley, E. Granstrom, and C. D. Frisbie, *Adv. Mater.* **11**, 261 (1999).
29. L. S. C. Pingree, O. G. Reid, and D. S. Ginger, *Adv. Mater.* **21**, 19 (2009).
30. B. B. Alba Avila, *Crit. Rev. Solid State Mater. Sci*. **35**, 38 (2010).
31. J. Liang and G. Scoles, *J. Phys. Chem. C* **114**, 10836 (2010).
32. M. E. Greene, C. R. Kinser, D. E. Kramer, L. S. C. Pingree, and M. C. Hersam, *Microsc. Res. Tech*. **64**, 415 (2004).
33. I. R. Lewis and H. G. M. Edwards, *Handbook of Raman Spectroscopy: From the Research Laboratory to the Process Line*, CRC Press, New York (2001).
34. A. Kudelski, *Talanta* **76**, 1 (2008).
35. Z. Movasaghi, S. Rehman, and I. U. Rehman, *Appl. Spectrosc. Rev.* **42**, 493 (2007).
36. W. L. Peticolas, *Biochimie* **57**, 417 (1975).
37. S. Das, *Chem. Geol*. **290**, 101 (2011).
38. D. Bersani and J. M. Madariaga, *J. Raman Spectrosc*. **43**, 1523 (2012).
39. E. V. Efremov, F. Ariese, and C. Gooijer, *Anal. Chim. Acta* **606**, 119 (2008).
40. B. Pettinger, P. Schambach, C. J. Villagómez, and N. Scott, *Annu. Rev. Phys. Chem*. **63**, 379 (2012).
41. S. Pahlow, A. März, B. Seise, K. Hartmann, I. Freitag, E. Kämmer, R. Böhme, V. Deckert, K. Weber, D. Cialla, and *J. Popp, Eng. Life Sci.* **12**, 131 (2012).
42. P. L. Stiles, J. A. Dieringer, N. C. Shah, and R. P. Van Duyne, *Annu. Rev. Anal. Chem*. **1**, 601 (2008).